AGU PUBLICATIONS

JGR

Journal of Geophysical Research: Atmospheres

RESEARCH ARTICLE
10.1002/2017JD027310

Key Points:
- Warm precipitation was found to be triggered too easily and too frequently in state-of-the-art global climate models
- Biases in cloud microphysics properties compensate partly for the too-easy formation of warm rain
- Better representation of autoconversion process and subgrid effects was found to improve warm rain simulation in some aspects

Correspondence to:
X. Jing and K. Suzuki,
jing_xw@aori.u-tokyo.ac.jp;
ksuzuki@aori.u-tokyo.ac.jp

Citation:
Jing, X., Suzuki, K., Guo, H., Goto, D., Ogura, T., Koshiro, T., & Mülmenstädt, J. (2017). A multimodel study on warm precipitation biases in global models compared to satellite observations. *Journal of Geophysical Research: Atmospheres*, *122*, 11,806–11,824. https://doi.org/10.1002/2017JD027310

Received 16 JUN 2017
Accepted 18 OCT 2017
Accepted article online 23 OCT 2017
Published online 11 NOV 2017

A Multimodel Study on Warm Precipitation Biases in Global Models Compared to Satellite Observations

Xianwen Jing[1], Kentaroh Suzuki[1], Huan Guo[2], Daisuke Goto[3], Tomoo Ogura[3], Tsuyoshi Koshiro[4], and Johannes Mülmenstädt[5]

[1]Atmosphere and Ocean Research Institute, University of Tokyo, Kashiwa, Japan, [2]UCAR CPAESS, NOAA Geophysical Fluid Dynamics Laboratory, Princeton, NJ, USA, [3]National Institute for Environmental Studies, Tsukuba, Japan, [4]Meteorological Research Institute, Japan Meteorological Agency, Tsukuba, Japan, [5]Institute for Meteorology, Universität Leipzig, Leipzig, Germany

Abstract The cloud-to-precipitation transition process in warm clouds simulated by state-of-the-art global climate models (GCMs), including both traditional climate models and a high-resolution model, is evaluated against A-Train satellite observations. The models and satellite observations are compared in the form of the statistics obtained from combined analysis of multiple-satellite observables that probe signatures of the cloud-to-precipitation transition process. One common problem identified among these models is the too-frequent occurrence of warm precipitation. The precipitation is found to form when the cloud particle size and the liquid water path (LWP) are both much smaller than those in observations. The too-efficient formation of precipitation is found to be compensated for by errors of cloud microphysical properties, such as underestimated cloud particle size and LWP, to an extent that varies among the models. However, this does not completely cancel the precipitation formation bias. Robust errors are also found in the evolution of cloud microphysical properties from nonprecipitating to drizzling and then to raining clouds in some GCMs, implying unrealistic interaction between precipitation and cloud water. Nevertheless, auspicious information is found for future improvement of warm precipitation representations: the adoption of more realistic autoconversion scheme in the high-resolution model improves the triggering of precipitation, and the introduction of a sophisticated subgrid variability scheme in a traditional model improves the simulated precipitation frequency over subtropical eastern ocean. However, deterioration in other warm precipitation characteristics is also found accompanying these improvements, implying the multisource nature of warm precipitation biases in GCMs.

1. Introduction

Precipitation is of great hydrological and radiative importance in the climate system by its depletion of cloud water and its modification to cloud optical properties (Intergovernmental Panel on Climate Change, 2013; Pincus & Baker, 1994). Precipitation also responds strongly to atmospheric conditions such as aerosol perturbations and global warming (Held & Soden, 2006; Hulme et al., 1998; Lebo & Feingold, 2014; L'Ecuyer et al., 2009; Mann et al., 2014; Sorooshian et al., 2009). The proper representation of precipitation process in global climate models (GCMs) therefore is crucial not only for realistic simulations of present climate but also, and more importantly, for reliable projections of future climate change due to human activities (Golaz et al., 2011; Golaz et al., 2013; Stephens, 2005).

Microphysical processes of precipitation are composed of two major processes, that is, the collision-coalescence among smaller cloud particles to form larger particles and a continuous broadening of particle size spectrum due to the condensational growth. However, given the coarse spatial resolution adopted in GCMs, these processes occurring at a cloud scale need to be represented in GCMs by "bulk parameterizations" in a highly approximated manner. These parameterizations represent the onset of precipitation by the so-called "autoconversion" process that accounts for the rain formation through collision and coalescence of cloud particles; the precipitation water thus formed further depletes cloud water through the "accretion" process. Although this type of parameterization is widely used in GCMs and efforts have been devoted to the sophistication of these parameterizations for decades (Berry, 1968; Kessler, 1969; Khairoutdinov & Kogan, 2000; Liu et al., 2007; Tripoli & Cotton, 1980), it is still subject to large uncertainties (Penner et al., 2006; Quaas et al., 2009).

Such uncertainty of parameterizations causes key discrepancies in precipitation behaviors of GCMs from the real atmosphere. One issue that has been pointed out is a common overestimate of the frequency of light rain compared with that inferred from satellite observations (Michibata et al., 2016; Stephens et al., 2010; Suzuki et al., 2015). Stephens et al. (2010) demonstrated that precipitation in weather prediction models and climate models, as well as high-resolution cloud-resolving models, occurred too often and was too light compared to those in satellite observations. With the aid of a simplified warm rain model as well as satellite observations and GCMs, such precipitation bias was also shown to reflect, at least in part, fundamental behaviors of autoconversion schemes adopted in GCMs (Suzuki et al., 2015). Michibata et al. (2016) further proposed that the overestimate of light rain can be a cause of unrealistically strong dependence of liquid water path (LWP) on perturbed aerosols, which is a critical pathway through which anthropogenic aerosol emissions influence the future climate change. Despite this progress in understanding model precipitation behaviors in light of satellite observations, the source of the precipitation biases is still somewhat obscure and thus requires more thorough investigations.

To identify the source of warm precipitation biases and fundamentally improve the model representation of precipitation, there is a growing interest in the GCM community to study precipitation and relevant processes with a particular emphasis on their process-level characteristics (Baker & Peter, 2008; Geoffroy et al., 2008; Takahashi et al., 2017; Zhao et al., 2016). This emerging trend of research is also facilitated by recent progress of satellite observations, particularly given the emergence of the A-Train constellation that simultaneously observes clouds and precipitation with multiple platforms and sensors (L'Ecuyer & Jiang, 2010; Stephens et al., 2008). This has provided an unprecedented opportunity to investigate process-level characteristics of cloud microphysics on the global scale. Particularly notable is the fact that key cloud properties, such as radar reflectivity, cloud particle size, and cloud top temperature, are detected or retrieved simultaneously along the A-Train orbits. These coobserved properties were then combined and exploited to observationally diagnose key aspects of the fundamental processes in cloud-to-precipitation transition (e.g., Suzuki et al., 2010; Wang et al., 2012). For instance, Suzuki et al. (2010) and Nakajima et al. (2010) proposed a method that combines the multiple-satellite observables in a particular manner to construct the statistics, named Contoured Frequency by Optical Depth Diagram (CFODD), which "fingerprint" the transition of vertical microphysical structure classified according to cloud particle sizes. The unique information of the precipitation process thus obtained from satellite observations has enabled us to evaluate and improve model parameterizations at a novel, fundamental level. Theoretical studies by Suzuki et al. (2013) and Suzuki et al. (2015) compared the satellite-observed and GCM-simulated characteristics of the CFODD statistics to expose a key discrepancy between them and interpreted it in the context of fundamental behaviors of autoconversion process representations in GCMs.

This study builds upon the previous studies (Suzuki et al., 2013, 2015) that developed the A-Train-based metrics for warm rain process and extends them to evaluations of up-to-date versions of multiple state-of-the-art climate models. Compared to these previous studies, this study focuses more on the evolution of cloud microphysical properties associated with precipitation process. The models are evaluated in their representations of the cloud-to-precipitation transition process of warm clouds (i.e., clouds with cloud top temperature$>$0°C) that are represented with varying cloud microphysics parameterizations. One particular objective of this study is to identify the source of biases in the warm precipitation process in GCMs in the context of the occurrence frequency of precipitation and the microphysical transition from cloud to rain. Another goal of this study is to explore the effects of key cloud microphysical parameterizations (such as autoconversion schemes and subgrid variabilities), which vary from model to model, on behaviors of the simulated warm rain. Given that the models examined include both traditional coarse-resolution and high-resolution GCMs, the multimodel comparisons provide a useful insight into possible effect of different spatial resolutions on the warm rain process representations. In the context of the scale dependency of the warm rain characteristics, we analyzed results from a traditional GCM framework with different precipitation schemes and representations of subgrid cloud water variabilities, which influence the onset and microphysical process rates of the warm rain formation (Lebsock et al., 2013; Morrison & Gettelman, 2008). Effects of the choice of cloud microphysical schemes are also investigated within the framework of the high-resolution model through sensitivity experiments with different autoconversion schemes.

This paper is organized as follows. Section 2 describes observational and model data used in this study. In section 3, we present the model biases identified in warm precipitation frequency and their relationship to cloud microphysical properties. Further examinations of the warm precipitation process are provided in section 4, where sources of the precipitation biases are investigated in terms of two aspects comprising the biases, that is, the errors in cloud microphysical properties and those in precipitation parameterizations. At last, the main findings of this study are summarized in section 5.

2. Data

2.1. A-Train Observations

The observation data used are satellite products of CloudSat and the Moderate Resolution Imaging Spectroradiometer (MODIS), both members of the A-Train constellation.

CloudSat carries a 94 GHz nadir-pointing radar that is capable of detecting the vertical profile of clouds and precipitation. The radar reflectivity of the 2B-GEOPROF product (Marchand et al., 2008) is used in this study. The radar reflectivity is sensitive to particle sizes within the radar beam and thus can be used to distinguish between cloud droplets and precipitation drops and to detect drizzle or light rain (Berg et al., 2010). In this study, we categorize radar profiles into three precipitation categories according to the profile maximum reflectivity (denoted as Z_{max}): nonprecipitating "cloud" with $-30 < Z_{max} < -15$ dBZ, "drizzle" with $-15 < Z_{max} < 0$ dBZ, and "rain" with $Z_{max} > 0$ dBZ (e.g., Haynes et al., 2009; Suzuki et al., 2015).

The Aqua MODIS collection 6 level 2 products (MYD06_L2) of effective cloud top particle radius (R_{eff}), cloud top temperature (T_c), and optical thickness (τ_c) (Platnick et al., 2015) are also employed. The R_{eff} and τ_c are retrieved at a spatial resolution of 1 km, and T_c is retrieved at a resolution of 5 km. The MODIS data are collocated to the CloudSat footprint to enable coanalysis of these two satellites. The January observations from 2007 to 2010 for both CloudSat and MODIS are used in our analysis.

A subset of observational data set is constructed by averaging cloudy pixels in the original A-Train data over every ~14 km along track, in order to facilitate the comparison between the fine-resolution observation and relatively coarse resolution of Nonhydrostatic ICosahedral Atmospheric Model (NICAM) (with grid size of ~14 km). This new data set is denoted as A-Train(14 km) in the following sections. Unless stated otherwise, the NICAM results should be evaluated by comparisons to A-Train(14 km). For traditional GCMs, since cloud simulators that generate subgrid cloud structures comparable with the original satellite detections are incorporated (see section 2.2), the results from the original A-Train data set are used as reference.

2.2. Model Simulations

The GCMs analyzed here are (1) the Geophysical Fluid Dynamics Laboratory Atmospheric Model version 3 (GFDL AM3) model incorporating a unified turbulence and cloud parameterization called the Cloud Layers Unified by Binormals (CLUBB) parameterization (denoted as GFDL_CLUBB) (Guo et al., 2014, 2015); (2) the new-generation GFDL Atmospheric Model version 4 (AM4) (denoted as GFDL_AM4) (Zhao et al., 2016, personal communication); (3) the global aerosol-climate model developed by the Max Planck Institute for Meteorology and the HAMMOZ consortium, version ECHAM6.1-HAM2.2-MOZ0.9 (denoted as ECHAM-HAMMOZ) (Lohmann et al., 2007; Zhang et al., 2012); (4) the Model for Interdisciplinary Research on Climate, version 5.2 (denoted as MIROC5.2) (Watanabe et al., 2010); (5) the Japan Meteorological Agency/Meteorological Research Institute Coupled Atmosphere-Ocean General Circulation Model version 3 (denoted as MRI-CGCM3) (Yukimoto et al., 2011, 2012) under improvement toward the Coupled Model Intercomparison Project Phase 6; (6) the global high-resolution model Nonhydrostatic ICosahedral Atmospheric Model (NICAM) (Satoh et al., 2008, 2014) with the autoconversion scheme of Berry (1968) (hereinafter BR68) (denoted as NICAM_Br); and (7) the NICAM model with the autoconversion scheme of Khairoutdinov and Kogan (2000) (hereinafter KK00) (denoted as NICAM_KK). The first five models are traditional coarse-resolution GCMs, while the last two (the two versions of NICAM) are global high-resolution models with horizontal resolutions of about 14 km. A summary of the model configurations is provided in Table 1.

Since the aim of this study is process-level investigation of model biases, the analysis here is based on 1 month (January) outputs, following a spin-up of 3 months or several years, from each of these models, with an output frequency of every 6 h. It was testified (not shown here) that it has little effect on the process-level

Table 1
Summary of Model Configurations

	Horizontal resolution	Number of subcolumns	Cloud schemes	Autoconversion schemes	Subgrid representation
GFDL_CLUBB	~1.0° × 1.0°	25	two moments	Khairoutdinov and Kogan (2000)	CLUBB, unified treatment
GFDL_AM4	~1.0° × 1.0°	25	two moments	Tripoli and Cotton (1980)	—
ECHAM-HAMMOZ	1.875° × 1.875°	100	two moments	Khairoutdinov and Kogan (2000)	—
MRI-CGCM3	1.125° × 1.125°	120	two moments	Tripoli and Cotton (1980)	—
MIROC5.2	1.4° × 1.4°	25	two moments	Berry (1968)	—
NICAM_Br	~14 km	—	two moments	Berry (1968)	—
NICAM_KK	~14 km	—	two moments	Khairoutdinov and Kogan (2000)	—

diagnostics that only 1 month outputs are used and whether prescribed sea surface temperature or a coupled ocean model is used. The model output is not sampled to match the A-Train observation times. The test using model output at one specific time of the day suggests that time sampling does not change the main findings of this study.

For comparisons with A-Train satellite observations, radar simulators are incorporated in all these models to transform model cloud profiles into radar reflectivity. The Cloud Feedback Model Intercomparison Project Observation Simulation Package (Bodas-Salcedo et al., 2011) is applied to the traditional GCMs, with the maximum-random overlap assumption for clouds at different vertical layers (Webb et al., 2001) and subgrid precipitation distribution algorithm of Zhang et al. (2010). The Joint Simulator for Satellite Sensors (J-simulator) (Hashino et al., 2013; Roh & Satoh, 2014; Satoh et al., 2016) that features fast computation with large size of model input is applied to NICAM for forward simulations of the satellite observables. For the traditional GCMs, our analyses are conducted for the subcolumn representations of grid-resolving, large-scale clouds (excluding convective clouds represented by cumulus parameterizations) as large-scale clouds are generated from typical bulk parameterizations of autoconversion and accretion. Whereas, as there is no partition between large-scale and convective clouds in NICAM, and it is virtually impossible to separate the two types of clouds from satellite observations, we use data of all warm clouds for NICAM and A-Train. We also restrict the analysis to oceanic areas, which will minimize the effects from different representations of aerosol-precipitation interactions among GCMs, as well as the uncertainties in satellite retrievals due to surface albedo and topographical uncertainties.

GFDL_CLUBB and GFDL_AM4 share the same model framework but differ in both precipitation schemes and representation of subgrid variability of condensate (Table 1). GFDL_CLUBB takes into account the subgrid variability of condensates as an important factor that enhances the autoconversion and accretion rates through a probability density function (PDF)-based method with unified treatment of subgrid dynamics. In GFDL_AM4, however, subgrid cloud variabilities are not considered in the autoconversion and accretion parameterizations. The comparisons of the two versions of the GFDL models thus demonstrate the joint effect of precipitation schemes and subgrid representations of clouds on the formation of precipitation.

The two versions of NICAM have identical model structures but different autoconversion schemes. The KK00 and BR68 schemes, each implemented to NICAM, are characterized by significantly different precipitation time scales and therefore produce different vertical microphysical structures, as shown in previous studies (Michibata & Takemura, 2015; Suzuki et al., 2015). With the comparison between the two versions of NICAM, we intend to investigate how the choice of such different autoconversion schemes can lead to the cloud-to-precipitation transition processes and cloud microphysical properties in a common global model.

A variety of autoconversion schemes are adopted in the other GCMs analyzed. MIROC5.2 applies the BR68 scheme, the same as NICAM_Br; ECHAM-HAMMOZ applies the KK00 scheme (Zhang et al., 2012), the same as NICAM_KK and GFDL_CLUBB. MRI-CGCM3 and GFDL_AM4 both adopt the Tripoli and Cotton (1980) autoconversion scheme but use different particle size thresholds to trigger precipitation (7 μm for MRI-CGCM3 and 8.5 μm for GFDL_AM4). Intercomparisons among different models sharing the same autoconversion scheme hint at how the same autoconversion scheme behaves in different models in representation of the precipitation formation.

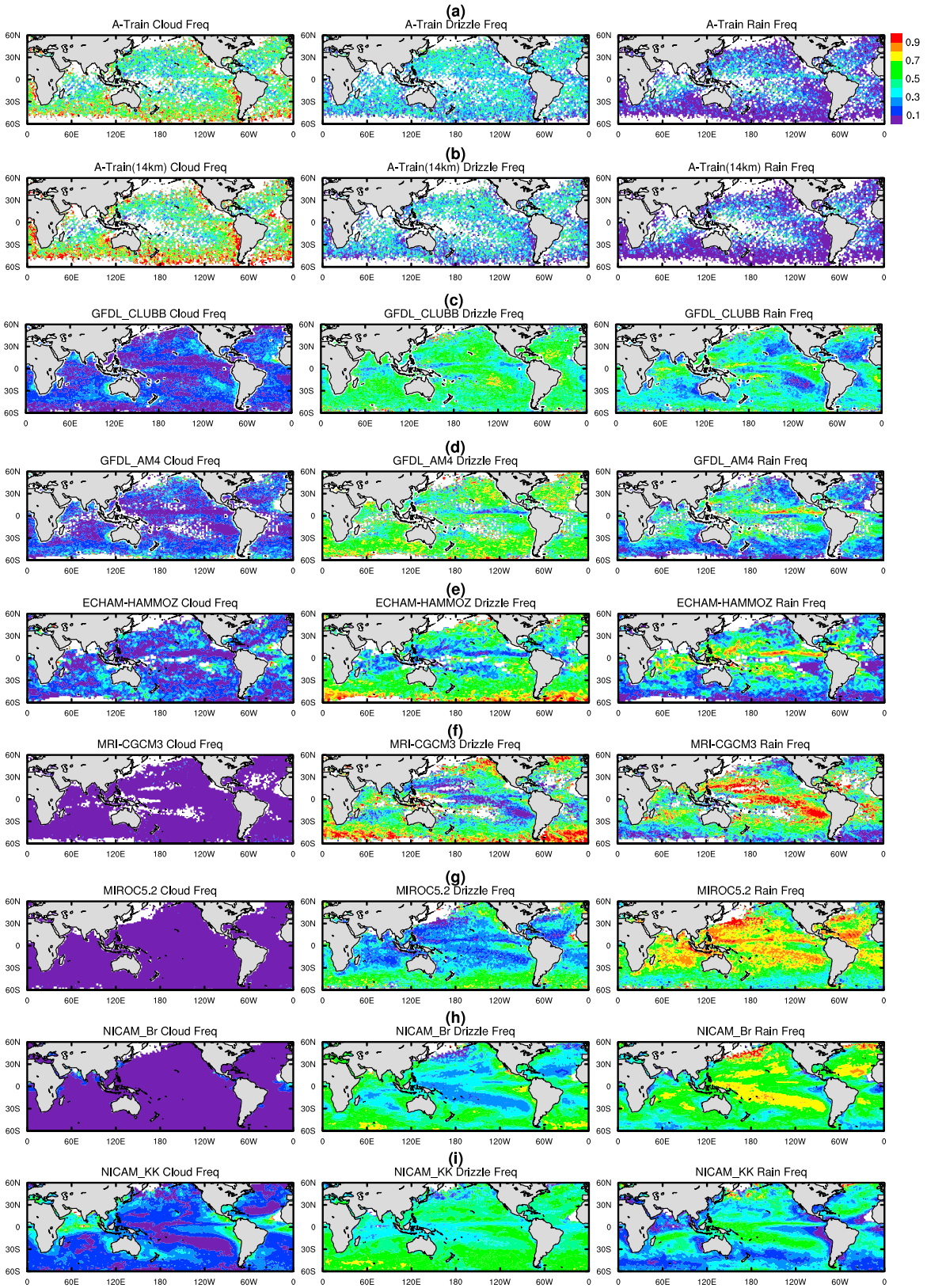

Figure 1. Distributions of in-cloud frequencies of cloud ($-30 < Z_{max} < -15$ dBZ, left), drizzle ($-15 < Z_{max} < 0$ dBZ, middle), and rain ($Z_{max} > 0$ dBZ, right), for (a) A-Train, (b) A-Train averaged every 14 km along track, (c) GFDL_CLUBB, (d) GFDL_AM4, (e) ECHAM-HAMMOZ, (f) MRI-CGCM3, (g) MIROC5.2, (h) NICAM_Br, and (i) NICAM_KK.

3. Precipitation Frequency Analysis

In this section, we evaluate the in-cloud frequency of cloud, drizzle, and rain, as defined based on radar reflectivity (section 2.1) and explore the connection between precipitation formation and cloud microphysical properties.

3.1. In-Cloud Precipitation Frequency

It has been reported that precipitation is generally too frequently generated in GCMs (Stephens et al., 2010; Suzuki et al., 2015). However, it has rarely been explicitly illustrated how frequent warm precipitation is generated from the in-cloud perspective. Here the occurrence frequencies of cloud, drizzle, and rain are defined from the in-cloud perspective as follows:

$$f_{\text{cloud}} = N_{\text{cloud}}/N_{\text{tot}} \tag{1}$$

$$f_{\text{drizzle}} = N_{\text{drizzle}}/N_{\text{tot}} \tag{2}$$

$$f_{\text{rain}} = N_{\text{rain}}/N_{\text{tot}} \tag{3}$$

where N_{cloud}, N_{drizzle}, and N_{rain} are the number of cloud, drizzle, and rain subcolumns (or pixels for A-Train) within each gridbox and N_{tot} is the total number of cloudy subcolumns ($N_{\text{tot}} = N_{\text{cloud}} + N_{\text{drizzle}} + N_{\text{rain}}$). The use of these in-cloud frequencies enables us to quantify how likely it is to drizzle or rain when clouds exist, and thus, it is straightforward to relate precipitation with cloud microphysics. These quantities are computed on 1.25°× 1.25° (latitude × longitude) grids from the A-Train orbit data and the NICAM data, whereas the original grid sizes are used for the traditional climate models (see Table 1).

Figure 1 shows the global geographical distributions of f_{cloud}, f_{drizzle}, and f_{rain} obtained from A-Train observations and various models between 60°S and 60°N. The globally averaged values are shown in Figure 2. The A-Train results (both the original and the 14 km averaged) (Figures 1a and 1b) suggest that for most regions, especially subtropical eastern oceans and midlatitude oceans, the majority of warm clouds are nonprecipitating; drizzling clouds constitute about 30–40% of all clouds in most regions, while raining clouds show notable occurrences only over the intertropical convergence zone. These characteristics of the in-cloud occurrence frequencies corroborate the fact that cloud-to-precipitation transition is both microphysically and dynamically controlled (Sorooshian et al., 2013). In terms of the global mean (Figure 2), it is fair to say that the majority of clouds (about 60%) are not precipitating and that most precipitating clouds are just drizzling.

However, all models show characteristics that are significantly different from the A-Train observations. The occurrences of nonprecipitating clouds are strikingly small, and those of drizzle and rain are substantially overpredicted in the models. The two versions of GFDL models (Figures 1c and 1d), ECHAM-HAMMOZ (Figure 1e), and NICAM_KK (Figure 1i) are slightly better than other models: nonprecipitating clouds occur relatively more frequently than in other models. It should be noted that the radar simulators used to generate subgrid radar reflectivity do not "see" the area fraction of precipitating clouds, and thus, when precipitation occurs in a grid box, all cloudy subcolumns contain precipitation. To take this "precipitation fraction" effect into account, we also calculated the observational cloud/precipitation frequencies from a grid-scale view: If any pixel in a 1.25° latitude segment is found to be raining, assume that all of the warm clouds in that segment are raining; otherwise, if any pixel in this segment is drizzling, assume all warm clouds are drizzling in that segment. The results (shown in Figure 2 as A-Train(gs)) suggest that the precipitation fraction effect does contribute partly to the overestimated precipitation frequency in Figures 1 and 2. However, the simulated precipitation frequencies are still remarkably larger than A-Train(gs). Therefore, the precipitation fraction effect cannot dismiss the fact that precipitation is generated too easily by GCMs. The too-easy generation of precipitation will also be demonstrated in the following sections.

A unique advantage of CLUBB is its representation of the subgrid variabilities of subtropical eastern oceanic stratus clouds (Guo et al., 2010, 2014, 2015). This is corroborated by the maximum f_{cloud} (Figure 1c, left) over these regions by GFDL_CLUBB. However, there is an obvious lack of midlatitude oceanic nonprecipitating

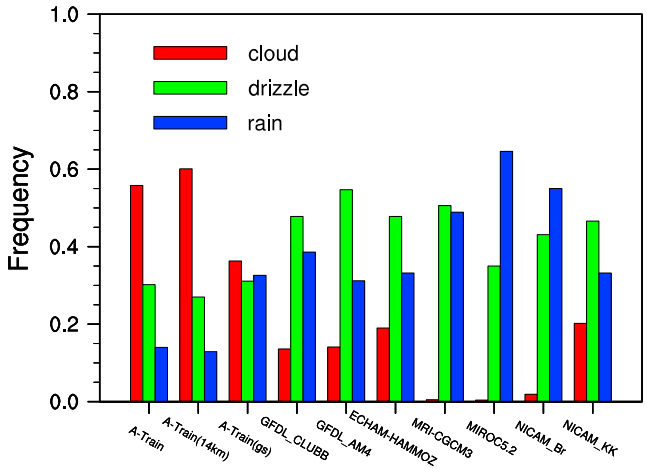

Figure 2. Relative frequency of cloud (f_{cloud}), drizzle ($f_{drizzle}$), and rain (f_{rain}) averaged between 60°S and 60°N for A-Train observations and model simulations. The observational results are calculated upon the original A-Train data set (A-Train), upon the subset A-Train data set averaged every 14 km along track (A-Train(14 km)), and from the grid-size (1.25° latitude along track) view by considering the precipitation fraction effect (A-Train(gs)).

clouds in GFDL_CLUBB, which are better represented by GFDL_AM4 (Figure 1d, left). These interesting differences imply that the dependencies of precipitation on subgrid variabilities of clouds and turbulences differ between subtropical eastern and midlatitude oceans.

On the other hand, the alteration of autoconversion schemes in NICAM also remarkably affects simulated f_{cloud}, $f_{drizzle}$, and f_{rain} as shown in Figures 1h and 1i. The increase of midlatitude and subtropical eastern oceanic clouds and the corresponding decrease of drizzle and rain in NICAM_KK are favorable. These features of NICAM_KK are quite similar to those of ECHAM_HAM (Figure 1e), which also uses the KK00 scheme to form warm precipitation.

As the definition of cloud, drizzle, and rain are based on radar reflectivity (Z_{max}), we compare the simulated and observed PDFs of subcolumn Z_{max} in Figure 3. The systematic overestimation of Z_{max} is found for all models. The A-Train Z_{max} peaks at around −25 dBZ (in the nonprecipitating cloud category), while those of models commonly peak at around 0 dBZ (in the drizzle or rain category). Even considering the uncertainty of radar reflectivity calculated by radar simulator to be up to 4–5 dBZ (Di Michele et al., 2012), the overestimation of radar reflectivity by GCMs is still robust.

3.2. Precipitation Occurrence Against Cloud Microphysics

The too-frequent occurrence of precipitation underlines that the water transition processes (i.e., the transition from cloud water to precipitation water) may not be correctly represented in GCMs. To evaluate the modeled water transition processes against observations, we computed fractional occurrences of different precipitation categories as a function of LWP (Kawamoto & Suzuki, 2012; Lebsock et al., 2008; L'Ecuyer et al., 2009; Suzuki et al., 2015), for both models and satellite observations. The observational LWP is calculated from MODIS R_{eff} and τ_c following Suzuki et al. (2015) as

$$\mathrm{LWP} = \frac{2}{3}\rho_w R_{\mathrm{eff}} \tau_c, \tag{4}$$

where ρ_w is the liquid water density.

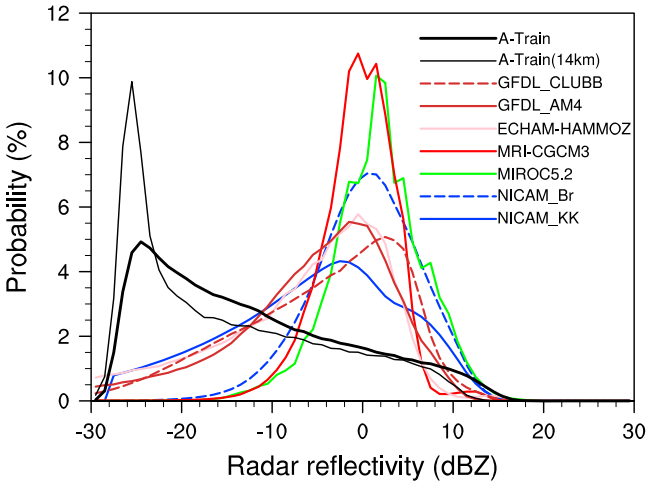

Figure 3. Probability density functions of subcolumn maximum radar reflectivity (Z_{max}) for A-Train observations and model simulations. A-Train represents the original satellite data, and A-Train(14 km) represents the subset data averaged every 14 km along track.

The results are shown in Figure 4. The A-Train results (Figures 4a and 4b) demonstrate that (1) the cloud-to-precipitation transition occurs more readily with increasing LWP, with the percentage of nonprecipitating clouds (rain) having its maximum (minimum) at the smallest LWP and decreasing (increasing) with increasing LWP, and (2) drizzle (which features smaller precipitating drop sizes) is responsible for most of the water transition over LWP below about 200 g m^{-2}, while rain (which features larger precipitating drop sizes) becomes dominant with further increase in LWP.

These observed characteristics are not properly captured by the GCMs as shown in Figures 4b–4h. The too small occurrence of nonprecipitating clouds and too large occurrence of precipitation at small LWP, compared to satellite observations, are found for all the models. This means that precipitation is triggered to form too easily in cloud development characterized by smaller LWP values. This, at least in part, explains why simulated precipitation is overly frequent, as shown in Figure 1. For GFDL_AM4 (Figure 4d) and ECHAM-HAMMOZ (Figure 4e), the magnitude and trend of the rain fraction (blue lines) with regard to LWP are more reasonably represented than those of other models. This implies that the drizzle to rain transition (represented primarily by accretion)

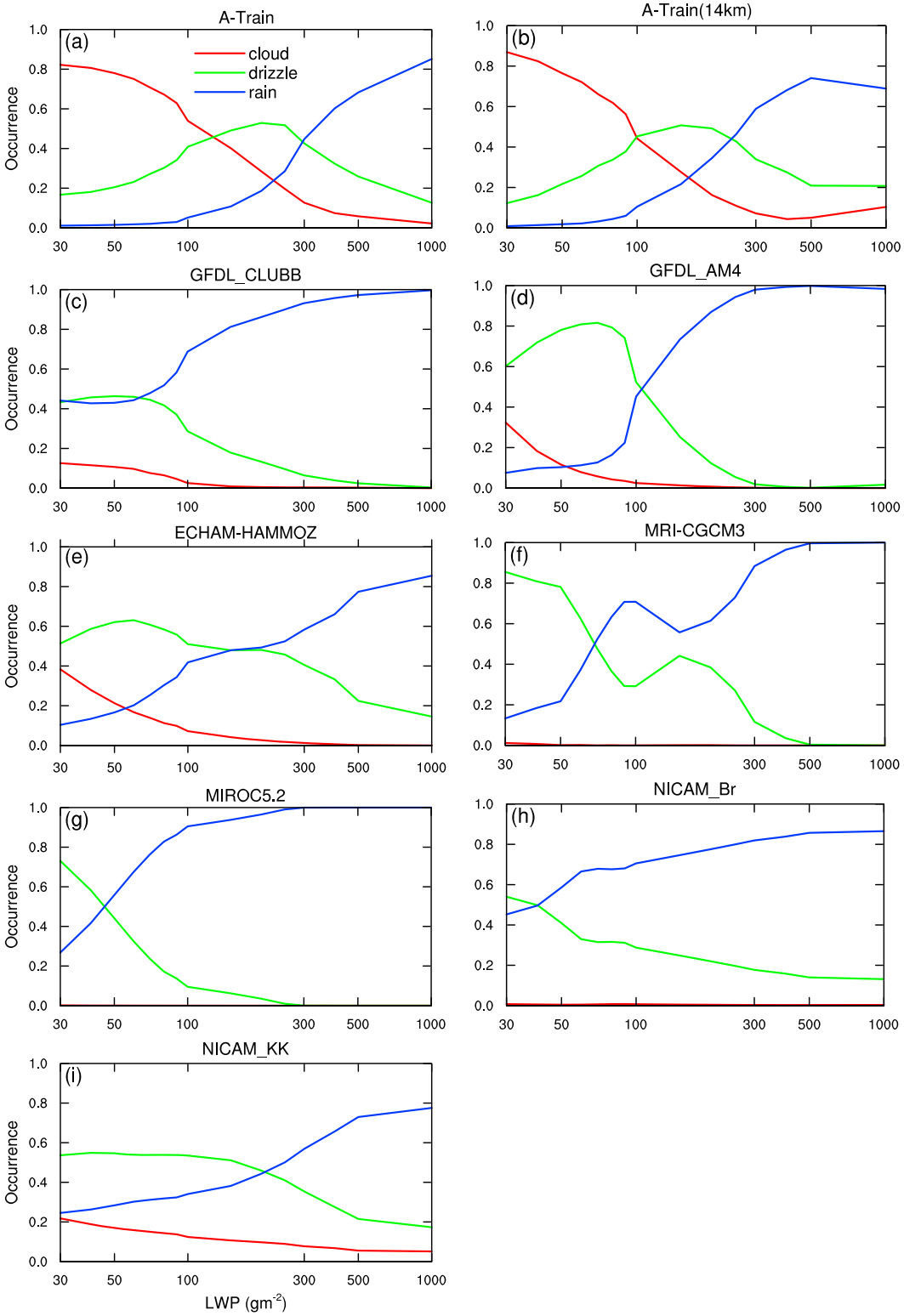

Figure 4. Fractional occurrence frequency of cloud (red), drizzle (green), and rain (blue) as a function of liquid water path for (a) A-Train, (b) A-Train averaged every 14 km along track, (c) GFDL_CLUBB, (d) GFDL_AM4, (e) ECHAM-HAMMOZ, (f) MRI-CGCM3, (g) MIROC5.2, (h) NICAM_Br, and (i) NICAM_KK.

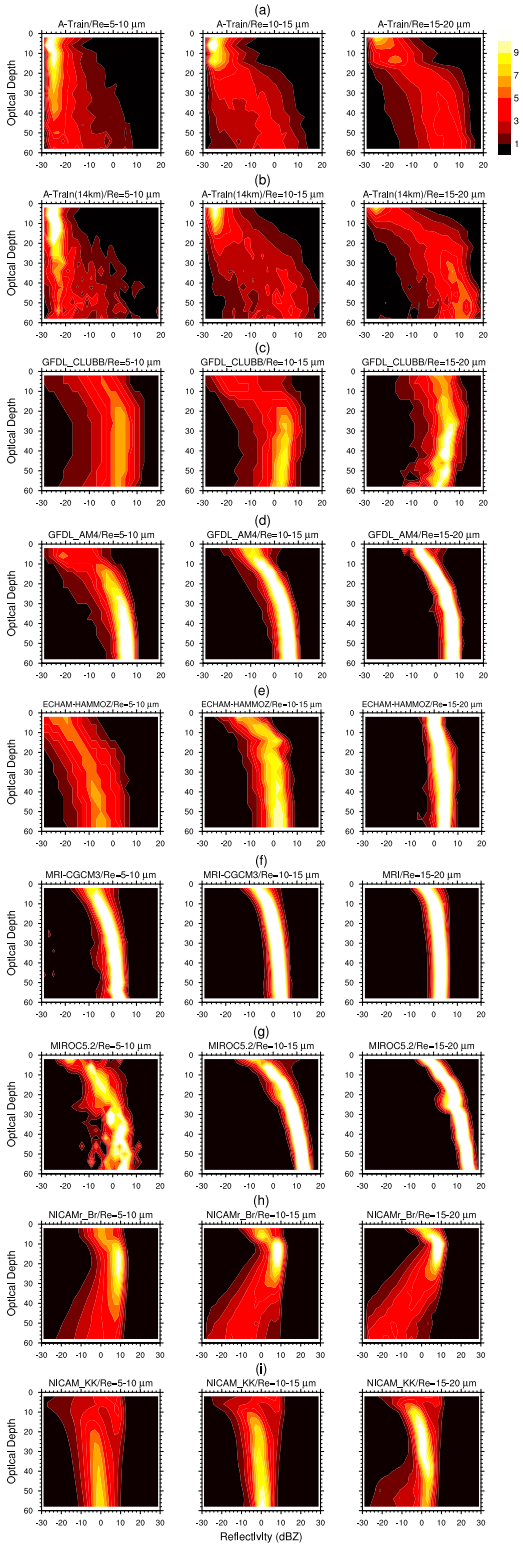

Figure 5. The probability function of radar reflectivity as a function of in-cloud optical depth (i.e., CFODDs) for (a) A-Train, (b) A-Train averaged every 14 km along track, (c) GFDL_CLUBB, (d) GFDL_AM4, (e) ECHAM-HAMMOZ, (f) MRI-CGCM3, (g) MIROC5.2, (h) NICAM_Br, and (i) NICAM_KK. The numbers of bins for optical depth and reflectivity are 15 and 25, respectively. The radar reflectivity is normalized in each bin of in-cloud optical depth.

appears to be reasonably represented and therefore that the transition from cloud to drizzle water (represented by autoconversion) is likely to be the primary cause for the overestimation of precipitation occurrence in these models. On the other hand, other models show a signature of too easily transition from drizzle to rainwater as well as from cloud to drizzle water, particularly for GFDL_CLUBB (Figure 4c) and NICAM_Br (Figure 4h), which show significantly large rain occurrences at the smallest LWP.

In addition to the water transition process investigated above, the vertical microphysical structure and its variation with respect to cloud top particle size provide us with a unique perspective to diagnose process-level biases in model representation of warm rain formation. The CFODD method of Suzuki et al. (2010, 2015) is employed to investigate this issue. In CFODD, vertical profiles of radar reflectivity are statistically represented on the in-cloud optical depth (ICOD) axis (rather than the traditional geometrical height axis), where occurrence frequencies of the radar reflectivity computed on each ICOD bin are displayed in the form of the contoured frequency diagram (Nakajima et al., 2010; Suzuki et al., 2010). For observations, vertical profile of ICOD is determined from the total MODIS τ_c with an adiabatic growth assumption algorithm (Suzuki et al., 2010). For models, ICOD is obtained from the model output of cloud optical depth profiles, and the radar reflectivity is obtained from the radar simulators.

Figure 5 shows the CFODDs obtained from A-Train observations and model simulations, classified according to R_{eff} into $5 < R_{\mathrm{eff}} \leq 10$ μm, $10 < R_{\mathrm{eff}} \leq 15$ μm, and $15 < R_{\mathrm{eff}} \leq 20$ μm. In A-Train (Figures 5a and 5b), the vertical structure shows a monotonic shift from nonprecipitating profiles to precipitating profiles with increasing R_{eff}: for $5 < R_{\mathrm{eff}} \leq 10$ μm, radar reflectivities throughout the cloud layer are mostly smaller than −15 dBZ; with the increase of R_{eff}, radar reflectivity at lower parts of clouds increases to a maximum of around 0 dBZ for $10 < R_{\mathrm{eff}} \leq 15$ μm, indicating the occurrence of drizzle, and to around 8 dBZ for $15 < R_{\mathrm{eff}} \leq 20$ μm, indicating the occurrence of rain. The shift of radar reflectivity structure with R_{eff} suggests either that the development of precipitation is accompanied by the growth of cloud top particle sizes or that precipitation is likely to form when cloud particle sizes exceed a critical value in a statistical sense.

However, all models exhibit a radar reflectivity over −15 dBZ even for $5 < R_{\mathrm{eff}} \leq 10$ μm as found in Figures 5c–5i, and the simulated radar reflectivity at small ICOD readily exceeds −15 dBZ for most models except ECHAM-HAMMOZ (Figure 5e). This suggests that precipitation is triggered too easily in models even when clouds are at incipient development stages in terms of both particle size and optical depth. This is consistent with the fact that precipitation readily occurs even when LWP is small as discussed above.

The difference between GFDL_CLUBB and GFDL_AM4, primarily in the subgrid variability of cloud water and turbulence (Guo et al., 2014), appears as the difference in the enhancement factor on autoconversion rate. This is depicted by the fact that the CFODDs of GFDL_CLUBB (Figure 5c) show notably different characteristics from those of GFDL_AM4 (Figure 5d): the radar reflectivity of GFDL_CLUBB is larger at small ICOD, and there is an attenuation of radar reflectivity (implied

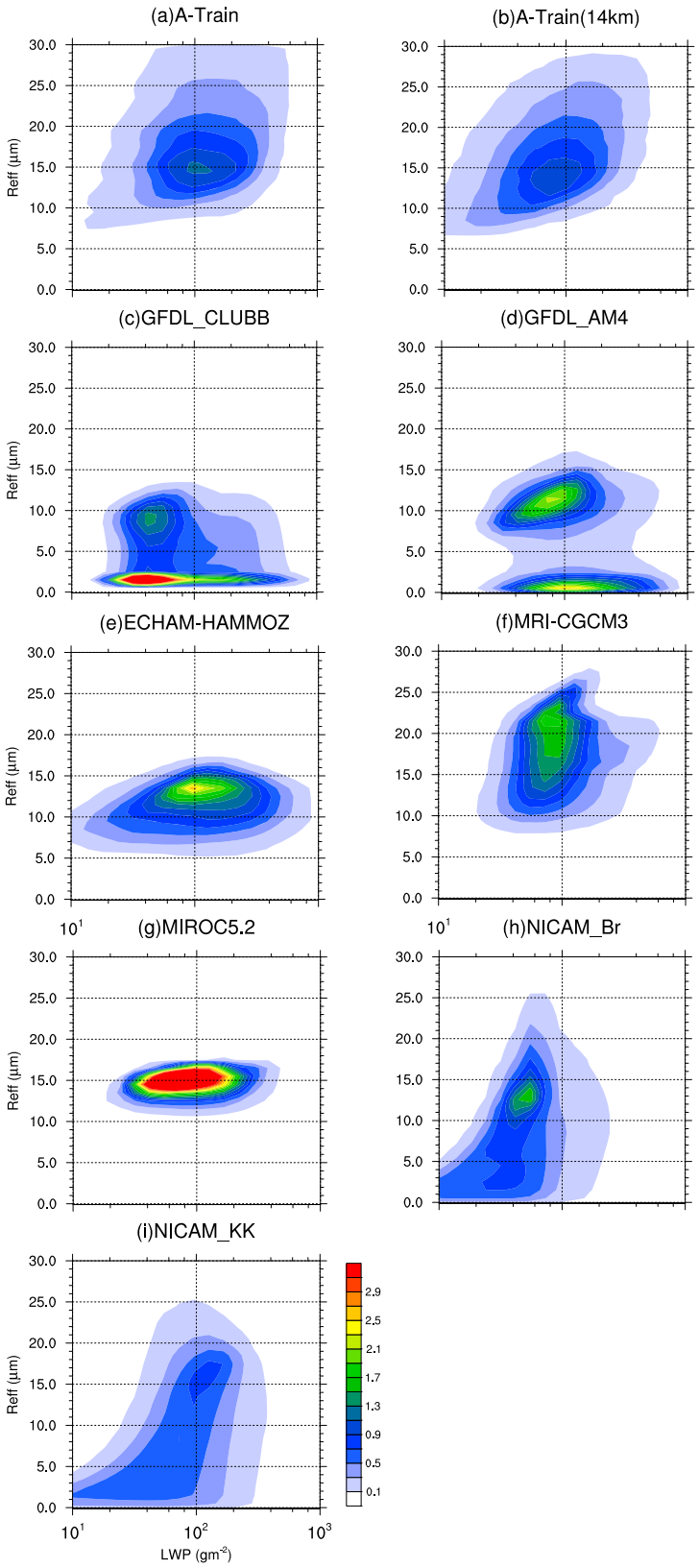

Figure 6. Two-dimensional probability density functions of cloud occurrence as a function of LWP and R_{eff} for (a) A-Train, (b) A-Train averaged every 14 km along track, (c) GFDL_CLUBB, (d) GFDL_AM4, (e) ECHAM-HAMMOZ, (f) MRI-CGCM3, (g) MIROC5.2, (h) NICAM_Br, and (i) NICAM_KK.

Table 2
The Cloud Top Effective Radius (R_{eff}) and Liquid Water Path (LWP) Averaged Between 60°S and 60°N for A-Train Observations and Model Simulations

	A-Train	A-Train(14 km)	GFDL_CLUBB	GFDL_ AM4	ECHAM-HAMMOZ	MRI-CGCM3	MIROC5.2	NICAM_Br	NICAM_KK
R_{eff}	19.80	18.39	6.38	7.23	11.15	14.36	13.71	5.34	6.96
LWP	158.33	120.77	87.05	147.03	136.24	93.35	70.00	66.56	102.49

from the decrease of radar reflectivity with increasing ICOD) in the rightmost two R_{eff} ranges. This demonstrates that precipitation is more efficient in GFDL_CLUBB than in GFDL_AM4.

It is worth noting that the two versions of NICAM with different autoconversion schemes show significantly different CFODD characteristics. NICAM_Br (Figure 5h) shows great attenuation effect of radar reflectivity, implying that precipitation is substantially too efficient at upper parts of clouds. On the other hand, NICAM_KK (Figure 5i) shows auspicious improvements: radar reflectivity is more likely to be smaller than −15 dBZ when R_{eff} is small, at least at ICOD <30, and the attenuation effect is significantly reduced. These results propose that drizzle is more likely to be triggered later and the transition from cloud water to precipitation water is less efficient in NICAM_KK than in NICAM_Br. These characteristics of NICAM_KK are closer to those found in the A-Train observations and therefore deemed more realistic than those of NICAM_Br.

It is also of some interest to compare different models sharing the same (or similar) cloud-to-precipitation parameterizations. MIROC5.2, which uses the same autoconversion scheme as NICAM_Br, produces rain efficiently even when $5 < R_{eff} \leq 10$ μm (Figure 5g), a characteristic similar to that of NICAM_Br. On the other hand, ECHAM-HAMMOZ, based on the same autoconversion scheme as NICAM_KK, also shows behaviors similar to NICAM_KK: the rightward shift of radar reflectivity profiles with increasing R_{eff} is significant, and clouds with $5 < R_{eff} \leq 10$ μm are less likely to produce a radar reflectivity over 0 dBZ. It is nevertheless worth noting that differences between MIROC5.2 and NICAM_Br, as well as between ECHAM-HAMMOZ and NICAM_KK, are also nonnegligible, implying the significance of discrepancies in representations of processes other than microphysics, such as dynamic and thermodynamic processes.

The biases identified in vertical microphysical structure of GCMs corroborate the too fast productions of precipitation on one hand, and hint at how cloud microphysical properties, such as LWP and R_{eff}, are inadequately associated with the precipitation occurrence on the other hand. The latter aspect is further explored in the following section.

4. Exploration of Microphysical Biases

The analyses above indicate that the onsets of precipitation in all the models are substantially too easily: the model precipitation occurs when LWP and R_{eff} are smaller than those for observed precipitation. In this section, we explore this too-easy formation of precipitation in more depth from two aspects: (1) biases in base cloud microphysical properties (e.g., LWP and R_{eff}) in GCMs and (2) biases in the cloud-to-precipitation transition process.

4.1. Cloud Microphysical Properties

To investigate the first aspect of biases, Figure 6 shows the PDFs of cloud occurrence as a function of LWP and R_{eff}. It is shown that clouds in satellite observations (Figures 6a and 6b) exert LWP centered around 100 g m^{-2} and R_{eff} centered around 15 μm. However, model simulations (Figures 6c–6i) show PDFs quite different from Figures 6a and 6b. Clouds in most models tend to have substantially smaller LWP (GFDL_CLUBB, MRI-CGCM3, MIROC, NICAM_Br, and NICAM_KK) and R_{eff} (GFDL_CLUBB, GFDL_AM4, ECHAM-HAMMOZ, NICAM_Br, and NICAM_KK) than observations. This can also be found from the spatially averaged results, as shown in Table 2. Moreover, unlike the single-peaked R_{eff} in A-Train, GFDL_CLUBB and GFDL_AM4 show two separated peaks, one at $R_{eff} < 5$ μm and the other at a larger R_{eff} of around 10 μm.

Generally speaking, LWP and R_{eff} are mostly underestimated by GCMs. These underestimated cloud properties compensate, at least in part, for the error that precipitation forms at smaller LWP and R_{eff} values (as shown in Figures 4 and 5). The extent of the error compensation differs among the models analyzed, resulting in different occurrence proportions of cloud, drizzle, and rain, as shown in Figure 2. Nevertheless, in all the

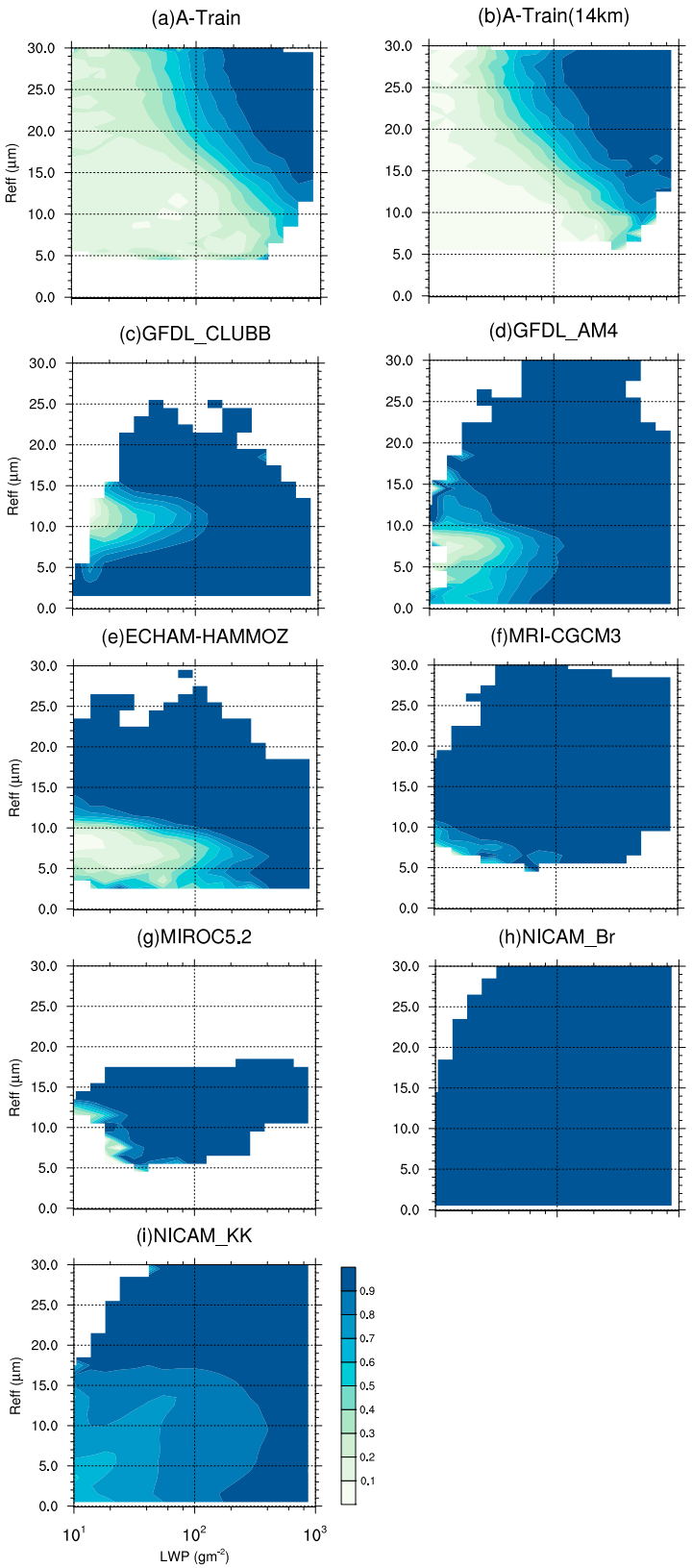

Figure 7. Occurrence frequency of precipitation (drizzle or rain) at each LWP and R_{eff} bin for (a) A-Train, (b) A-Train averaged every 14 km along track, (c) GFDL_CLUBB, (d) GFDL_AM4, (e) ECHAM-HAMMOZ, (f) MRI-CGCM3, (g) MIROC5.2, (h) NICAM_Br, and (i) NICAM_KK.

models examined, the too-efficient precipitation biases are not completely canceled by the cloud property biases, resulting in model precipitation that is still biased toward higher occurrence of precipitation.

It should be noted that the onset of precipitation (i.e., autoconversion) in GCMs is generally parameterized independently at each model layer, thus only liquid water content and cloud droplet size at a particular vertical layer work in the triggering of precipitation. However, as precipitation fluxes at a particular model layer typically rely on those at layers above, precipitation water also interacts with cloud water in its pathway through the accretion process. So the simulated LWP and R_{eff} shown above are an outcome of the layer-independent precipitation parameterization, and thus can be used as proxies for single-layer properties to indicate biases in models' precipitation process.

4.2. Precipitation Process

In addition to the base errors in liquid water path and cloud particle size, the dependence of precipitation formation on these cloud properties is another source of error that should be examined. Such a diagnosis is shown in Figure 7, which presents precipitation (drizzle or rain) occurrence frequency as a function of LWP and R_{eff}.

In the A-Train results (Figures 7a and 7b), the probability of precipitation monotonically increases with increasing LWP and R_{eff}, with its maximum at the right-upper corner of the diagram. The majority of the models, except for NICAM_Br, exhibit such a trend in a qualitative sense. Therefore, the precipitation formation processes in these models possess realistic behavior at least qualitatively.

However, GFDL models (particularly GFDL_CLUBB) (Figures 7c and 7d) also exert an increasing trend in the right-lower direction found at the lower part of the diagrams, implying that precipitating clouds can have smaller R_{eff} than that of nonprecipitating clouds. This is an unrealistic relationship not identified in satellite observations.

MRI-CGCM3 (Figure 7f) and MIROC (Figure 7g) show substantially more frequent precipitation than most other models. Even with consideration of the given base errors of LWP and R_{eff} shown in Figures 6f and 6g, the onset of precipitation in MRI-CGCM3 and MIROC occurs still too easily. This suggests that the too-frequent precipitation biases exposed in these two models are attributed to the precipitation formation parameterization that relates the precipitation occurrence with cloud properties.

More realistic statistics are shown in Figure 7i for NICAM_KK particularly when compared with Figure 7h for NICAM_Br. The incorporation of the KK00 autoconversion scheme in NICAM makes the triggering of precipitation much more realistic than that using the BR68 scheme. However, NICAM_KK still triggers precipitation too easily (at too small R_{eff} and LWP); thus, the precipitation frequency in NICAM_KK is still highly overestimated as shown in Figures 1i and 2.

To further investigate the relationship between the precipitation process and each cloud property (R_{eff} or LWP), Figures 8 and 10 show the box-and-whisker plots of R_{eff} and LWP, respectively, for different precipitation categories.

It is shown in Figures 8a and 8b that R_{eff} increases steadily from the cloud category to the rain category in satellite observations. This means that the development of precipitation is accompanied with the enlargement of cloud particle sizes. Some models, such as ECHAM-HAMMOZ (Figure 8e), MRI-CGCM3 (Figure 8f), and MIROC5.2 (Figure 8g), capture this trend although the exact R_{eff} ranges in the simulations are not necessarily comparable to those of observations. Among these models, MRI-CGCM3 is quantitatively closer to observations than other models.

However, the two versions of GFDL models (Figures 8c and 8d) and NICAM_KK (Figure 8i) fail to represent the increase of R_{eff} with the enhancement of precipitation. In GFDL_AM4 and NICAM_KK, an increase of R_{eff} from the cloud category to the drizzle category is found, but the R_{eff} of the rain category is comparable to, if not slightly smaller than, that of the drizzle category. NICAM_Br behaves slightly better than NICAM_KK in terms of the continuously increasing R_{eff} from cloud to rain. Remarkably, GFDL_CLUBB shows a monotonic decrease of R_{eff} from cloud to rain categories, in contrast to the tendency in satellite observations.

The decreasing trend of R_{eff} might be associated with the too-efficient rain formation that depletes the cloud liquid water so efficiently. In two-moment cloud microphysics parameterizations, cloud particle size at each

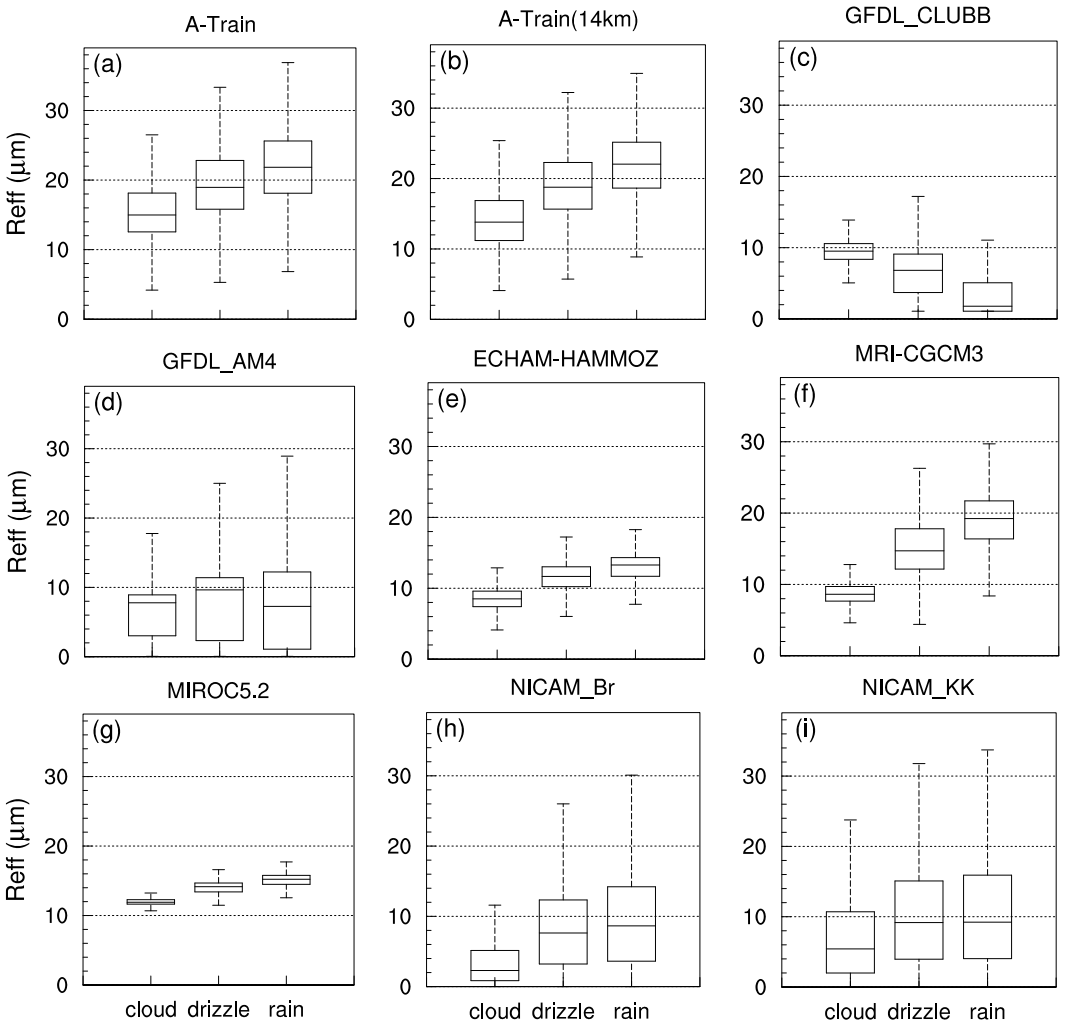

Figure 8. The box-and-whisker plots of R_{eff} for the cloud, drizzle, and rain modes for (a) A-Train, (b) A-Train averaged every 14 km along track, (c) GFDL_CLUBB, (d) GFDL_AM4, (e) ECHAM-HAMMOZ, (f) MRI-CGCM3, (g) MIROC5.2, (h) NICAM_Br, and (i) NICAM_KK.

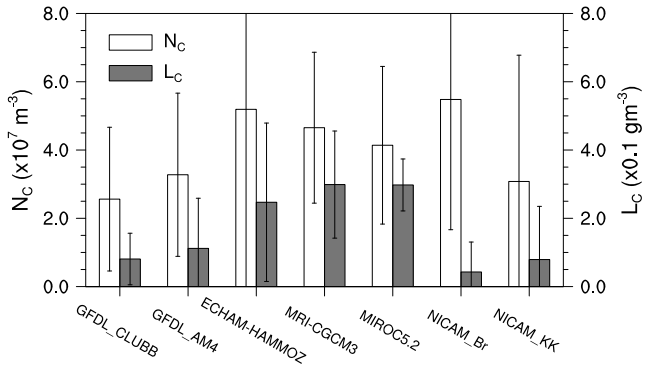

Figure 9. Averaged (60°S–60°N) cloud number concentration (N_c, white bars) and liquid water content (L_c, black bars) at cloud top simulated by models. The error bars represent the standard deviation.

grid cell (R_c) depends on both liquid water content (L_c) and cloud droplet number concentration (N_c, typically parameterized from aerosol activation) as $R_c \propto L_c^{1/3} N_c^{-1/3}$. As R_c depends on L_c and N_c, the variations of R_{eff} (a proxy for R_c) with precipitation enhancement somewhat reflect the precipitation-induced depletion of L_c and scavenging of aerosols that influences N_c. These changes of L_c and N_c induce competing effects on R_c: the precipitation-induced depletion of L_c and N_c operates to decrease and increase R_c, respectively. Given this dependency of R_c on L_c and N_c, the net decreasing tendency of R_{eff} with enhanced precipitation found in GFDL_CLUBB suggests that the L_c effect dominates over the N_c effect. The lack of increase in R_{eff} with precipitation in the GFDL and NICAM models (as shown in Figures 8c, 8d, 8h, and 8i) therefore implies that the cloud-to-precipitation transitions are so efficient (the autoconversion or accretion rate may be unrealistically large) that there remains less cloud water (L_c), leading to a reduction of the particle size. This is supported by

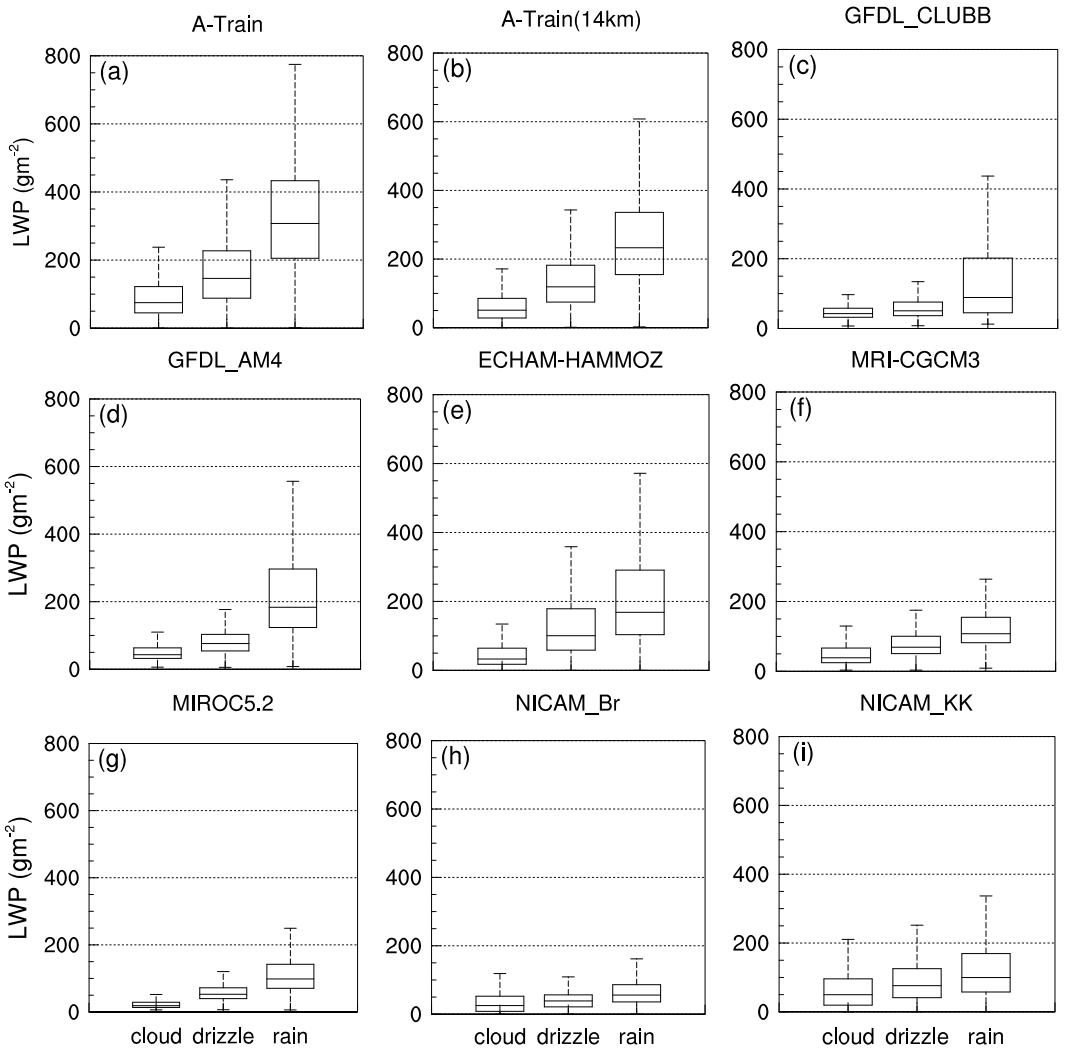

Figure 10. The same as Figure 8, but for LWP.

Figure 9, which shows L_c at cloud top is 2–7 times smaller for GFLD and NICAM models than for other models, while N_c at cloud top differs in much less extent.

Similar to Figures 8a and 8b, the A-Train statistics of LWP in Figures 10a and 10b also show a robust left-to-right increase, indicating that the enhancement of precipitation statistically coincides with more abundant cloud water. Most models reproduce this increasing trend of LWP, but with smaller values. It is interesting in this regard that the increase of LWP from the cloud category to the drizzle category is less significant in GFDL_CLUBB (Figure 10c). If we hypothesize that autoconversion is primarily responsible for the water transition from cloud to drizzle, and that accretion is primarily responsible for the water transition from drizzle to rain, then the inefficient growth of LWP from cloud to drizzle may imply that the autoconversion depletion of cloud water is too efficient in GFDL_CLUBB. However, it may also be a consequence of dynamical biases: the dynamically controlled vapor condensation may be insufficient for the LWP growth in the drizzle category of GFDL_CLUBB. This argument could be clarified by more detailed analysis in future studies.

The results of GFDL_AM4 (Figure 10d) and ECHAM-HAMMOZ (Figure 10e) resemble those of A-Train (Figure 10a) in both magnitude and trend, suggesting that their water transition processes are better represented than other models. This is consistent with what is shown in Figure 4. The behavior of LWP variations in MRI-CGCM3 (Figure 10f) and MIROC5.2 (Figure 10g) are at least qualitatively similar to the A-Train result, implying that the autoconversion and accretion efficiencies may be reasonably represented (on the basis of the hypothesis stated above).

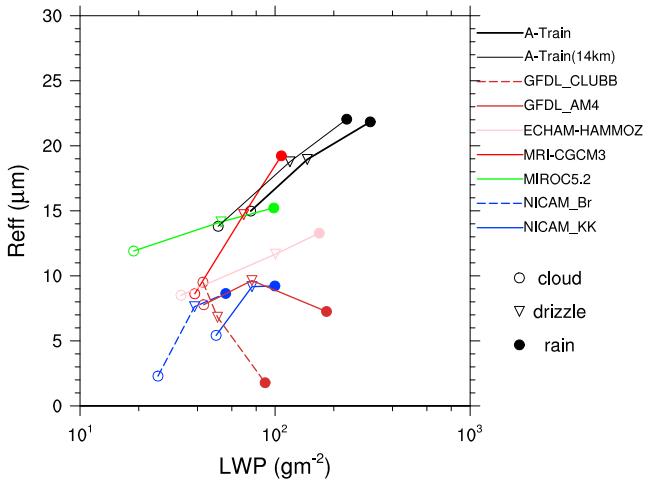

Figure 11. Transition of precipitation mode in the LWP-R_{eff} coordinates. The position of each mark represents the median values of R_{eff} and LWP as shown in Figures 8 and 10, respectively.

In NICAM, the LWP transition with enhancement of precipitation (Figures 10h–10i) is not as robust as shown in observations (Figure 10b). However, notable improvement by applying the KK00 autoconversion scheme (Figure 10i) is seen, illustrated by both the increased magnitude of LWP and also more robust increasing of LWP with the enhancement of precipitation compared with Figure 10h.

Figure 11 summarizes the behaviors of cloud water and particle size as a function of different precipitation occurrence shown in Figures 8 and 10 in the form of the median values of LWP and R_{eff} for each precipitation category in the LWP–R_{eff} coordinates. By connecting the marks for a single model or the observations, the transitions of cloud microphysical properties with changing precipitation are hinted. Figure 11, containing information on both cloud water transition and cloud occurrence statistics, is also a joint consequence of Figures 6 and 7.

In Figure 11, satellite observations show a right-upper trend from the cloud category to the rain category. Three models (ECHAM-HAMMOZ, MRI-CGCM3, and MIROC5.2) reproduce this trend although with the locations inconsistent with observations, highlighting the biases in simulated LWP and R_{eff}. For GFDL models, enhanced precipitation is associated with increasing LWP but decreasing R_{eff}, which is particularly the case in GFDL_CLUBB. For NICAM models, the increase of LWP with enhanced precipitation is found (although not as robust as shown in observations), but R_{eff} also hardly increases with precipitation enhancement. The differences in subgrid parameterizations (in the two versions of GFDL models) and autoconversion schemes (as identified from the comparisons between the two versions of NICAM models) pose substantial effects, but fundamental biases seem to exist that are responsible for the lack of increasing R_{eff} in GFDL and NICAM models.

The results described above provide a picture of model biases in representation of precipitation: although precipitation occurs too frequently in most GCMs, the precipitation process itself may still be reasonably simulated by some models (as inferred from cloud microphysical property transitions). Thus, two aspects of errors in precipitation parameterizations of GCMs should be considered separately. One is the "triggering" problem: in what condition should cloud water be transferred to precipitation water; the other is the "evolution" problem: how precipitation interacts with cloud water. The former appears to be critical for the "too-frequent" problems of simulated precipitation, while the latter can be critical for the cloud microphysical property biases associated with precipitation occurrence. Nevertheless, this does not dismiss the importance of the base biases in the parameterizations of cloud microphysical properties. Moreover, the coupling between cloud macrophysics and cloud microphysics can be another important source of warm precipitation biases, which is not examined here.

5. Conclusions

In this study, we evaluated the cloud-to-precipitation transition process simulated by up-to-date versions of multiple state-of-the-art GCMs, including both traditional climate models and a global high-resolution model, against A-Train satellite observations. We found that both traditional and high-resolution GCMs share some similarities in characteristics of simulated precipitation: all the analyzed models continue to have the problem of too-frequent formation of precipitation, similar to the previous versions of models. Precipitation was triggered even when cloud particle size and liquid water path were still too small, and thus, the occurrences of precipitation were significantly overestimated. The bulk precipitation schemes used in models play a crucial role in determining these simulated precipitation behaviors, regardless of the horizontal resolution of models. We also found that models contained "compensating errors" between cloud properties (LWP and R_{eff}) and the precipitation formation process: the too-efficient precipitation formations were partly compensated for by the systematic underestimates of LWP and R_{eff}. However, this compensation did not completely cancel the precipitation formation biases. Even with consideration of these systematic cloud property errors, precipitation was still generated too easily in the GCMs than inferred from the observations. This implied that there

were fundamental biases in representation of the precipitation onset in GCMs (e.g., autoconversion schemes and coupling between microphysics and macrophysics).

In addition to the problem in precipitation occurrence frequency, the evolution of cloud microphysical properties with the enhancement of precipitation was also found to suffer from robust errors. For instance, the GFDL models and NICAM models fail to represent an increase in cloud particle size, with enhanced occurrence of precipitation. Despite these model biases, useful insight into possible improvements of warm precipitation parameterization in GCMs was obtained from the analysis of this study. On one hand, the sensitivity test with NICAM revealed that the adoption of a more realistic autoconversion scheme significantly improved the triggering of precipitation. On the other hand, the use of the sophisticated subgrid scheme CLUBB, in addition to a more realistic autoconversion scheme, in the GFDL model brought notable improvement in the representation of subtropical eastern oceanic precipitation. These results underscore the importance of autoconversion and subgrid schemes for the improvement of warm precipitation representation. But deterioration of other precipitation characteristics accompanying these improvements implies that warm precipitation biases stem from multisources. Other aspects of models, both microphysics and macrophysics and also the coupling between them, are highly important for realistic representation of precipitation process. Therefore, the effect of implementing a particular autoconversion or subgrid scheme may be model-dependent.

Acknowledgments

This study was supported by NOAA's Climate Program Office's Modeling, Analysis, Predictions and Projections program with the grant NA15OAR4310153 and JAXA GCOM-C project. K.S. and T.O. are supported by the Integrated Research Program for Advancing Climate Models (TOUGOU program) from the Ministry of Education, Culture, Sports, Science and Technology (MEXT), Japan. The CloudSat data were obtained from the CloudSat Data Processing Center (DPC) at Colorado State University (http://www.cloudsat.cira.colostate.edu). The MODIS data were obtained from the Level-1 and Atmosphere Archive and Distribution System (LAADS) Distributed Active Archive Center (DAAC) of NASA (https://ladsweb.modaps.eosdis.nasa.gov). The model data are available from https://doi.org/10.5281/zenodo.890474. The ECHAM-HAMMOZ model is developed by a consortium composed of ETH Zurich, Max Planck Institut für Meteorologie, Forschungszentrum Jülich, University of Oxford, the Finnish Meteorological Institute, and the Leibniz Institute for Tropospheric Research and managed by the Center for Climate Systems Modeling (C2SM) at ETH Zurich. We thank Christine Nam and Jan Kretzschmar for help with COSP in ECHAM-HAMMOZ. The NICAM simulations were performed using the K computer at RIKEN in Japan (general use proposal numbers: 150156, 150288, 160004, 160231, and 170017). We would like to thank Jean-Christophe Golaz and Ming Zhao for their leadership in developing AM4 and the GFDL model development team for the permission of publishing AM4 results.

References

Baker, M. B., & Peter, T. (2008). Small-scale cloud processes and climate. *Nature*, *451*(7176), 299–300. https://doi.org/10.1038/nature06594

Berg, W., L'Ecuyer, T., & Haynes, J. M. (2010). The distribution of rainfall over oceans from spaceborne radars. *Journal of Applied Meteorology and Climatology*, *49*(3), 535–543. https://doi.org/10.1175/2009JAMC2330.1

Berry, E. X. (1968). Modification of the warm rain process, paper presented at 1st National Conference on Weather Modification (pp. 81–85). Albany, NY. American Meteorological Society, April 28–May 1.

Bodas-Salcedo, A., Webb, M. J., Bony, S., Chepfer, H., Dufresne, J. L., Klein, S. A., … John, V. O. (2011). COSP: Satellite simulation software for model assessment. *Bulletin of the American Meteorological Society*, *92*(8), 1023–1043. https://doi.org/10.1175/2011BAMS2856.1

Di Michele, S., Ahlgrimm, M., Forbes, R., Kulie, M., Bennartz, R., Janisková, M., & Bauer, P. (2012). Interpreting an evaluation of the ECMWF global model with CloudSat observations: Ambiguities due to radar reflectivity forward operator uncertainties. *Quarterly Journal of the Royal Meteorological Society*, *138*(669), 2047–2065. https://doi.org/10.1002/qj.1936

Geoffroy, O., Brenguier, J.-L., & Sandu, I. (2008). Relationship between drizzle rate, liquid water path and droplet concentration at the scale of a stratocumulus cloud system. *Atmospheric Chemistry and Physics*, *8*(16), 4641–4654. https://doi.org/10.5194/acp-8-4641-2008

Golaz, J.-C., Horowitz, L. W., & Levy, H. II (2013). Cloud tuning in a coupled climate model: Impact on 20th century warming. *Geophysical Research Letters*, *40*(10), 2246–2251. https://doi.org/10.1002/grl.50232

Golaz, J.-C., Salzmann, M., Donner, L., Horowitz, L., Ming, Y., & Zhao, M. (2011). Sensitivity of the aerosol indirect effect to subgrid variability in the cloud parameterization of the GFDL atmosphere general circulation model AM3. *Journal of Climate*, *24*(13), 3145–3160. https://doi.org/10.1175/2010JCLI3945.1

Guo, H., Golaz, J.-C., Donner, L. J., Ginoux, P., & Hemler, R. S. (2014). Multivariate probability density functions with dynamics in the GFDL atmospheric general circulation model: Global tests. *Journal of Climate*, *27*(5), 2087–2108. https://doi.org/10.1175/JCLI-D-13-00347.1

Guo, H., Golaz, J.-C., Donner, L. J., Larson, V. E., Schanen, D. P., & Griffin, B. M. (2010). Multi-variate probability density functions with dynamics for cloud droplet activation in large-scale models: Single column tests. *Geoscientific Model Development*, *3*(2), 475–486. https://doi.org/10.5194/gmd-3-475-2010

Guo, H., Golaz, J.-C., Donner, L. J., Wyman, B., Zhao, M., & Ginoux, P. (2015). CLUBB as a unified cloud parameterization: Opportunities and challenges. *Geophysical Research Letters*, *42*(11), 4540–4547. https://doi.org/10.1002/2015GL063672

Hashino, T., Satoh, M., Hagihara, Y., Kubota, T., Matsui, T., Nasuno, T., & Okamoto, H. (2013). Evaluating cloud microphysics from NICAM against CloudSat and CALIPSO. *Journal of Geophysical Research: Atmospheres*, *118*(13), 7273–7292. https://doi.org/10.1002/jgrd.505%2064

Haynes, J. M., L'Ecuyer, T., Stephens, G. L., Miller, S. D., Mitrescu, C., Wood, N. B., & Tanelli, S. (2009). Rainfall retrievals over the ocean with spaceborne high-frequency cloud radar. *Journal of Geophysical Research*, *114*, D00A22. https://doi.org/10.1029/2008JD009973

Held, I., & Soden, B. (2006). Robust responses of the hydrological cycle to global warming. *Journal of Climate*, *19*(21), 5686–5699. https://doi.org/10.1175/JCLI3990.1

Hulme, M., Osborn, T. J., & Johns, T. C. (1998). Precipitation sensitivity to global warming: Comparison of observations with HadCM2 simulations. *Geophysical Research Letters*, *25*(17), 3379–3382. https://doi.org/10.1029/98GL02562

Intergovernmental Panel on Climate Change (2013). *Climate change 2013* (p. 1535). The Physical Science Basis. Contribution of Working Group I to the Fifth Assessment Report of the Intergovernmental Panel on Climate Change, Cambridge, UK, and New York: Cambridge University Press.

Kawamoto, K., & Suzuki, K. (2012). Microphysical transition in water clouds over the Amazon and China derived from space-borne radar and radiometer data. *Journal of Geophysical Research*, *117*, D05212. https://doi.org/10.1029/2011JD016412

Kessler, E. (1969). *On the distribution and continuity of water substance in atmospheric circulations*, *Meteorological Monographs* (Vol. 32, p. 84). Boston, MA: American Meteorological Society. https://doi.org/10.1007/978-1-935704-36-2

Khairoutdinov, M., & Kogan, Y. (2000). A new cloud physics parameterization in a large-eddy simulation model of marine stratocumulus. *Monthly Weather Review*, *128*(1), 229–243. https://doi.org/10.1175/1520-0493(2000)128%3C0229:ANCPPI%3E2.0.CO;2

L'Ecuyer, T. S., Berg, W., Haynes, J., Lebsock, M., & Takemura, T. (2009). Global observations of aerosol impacts on precipitation occurrence in warm maritime clouds. *Journal of Geophysical Research: Atmospheres*, *114*, D09211. https://doi.org/10.1029/2008JD011273

Lebo, Z. J., & Feingold, G. (2014). On the relationship between responses in cloud water and precipitation to changes in aerosol. *Atmospheric Chemistry and Physics*, *14*(21), 11817–11831. https://doi.org/10.5194/acp-14-%2011817-2014

Lebsock, M., Morrison, H., & Gettelman, A. (2013). Microphysical implications of cloud-precipitation covariance derived from satellite remote sensing. *Journal of Geophysical Research*, *118*, 6521–6533. https://doi.org/10.1002/jgrd.50347

Lebsock, M., Stephens, G. L., & Kummerow, C. (2008). Multisensor satellite observations of aerosol effects on warm clouds. *Journal of Geophysical Research*, *113*, D15205. https://doi.org/10.1029/2008JD009876

L'Ecuyer, T. S., & Jiang, J. (2010). Touring the atmosphere aboard the A-Train. *Physics Today*, *63*(7), 36–41. https://doi.org/10.1063/1.3463626

Liu, Y., Daum, P. H., McGraw, R. L., Miller, M. A., & Niu, S. (2007). Theoretical expression for the autoconversion rate of the cloud droplet number concentration. *Geophysical Research Letters*, *34*, L16821. https://doi.org/10.1029/2007GL030389

Lohmann, U., Stier, P., Hoose, C., Ferrachat, S., Kloster, S., Roeckner, E., & Zhang, J. (2007). Cloud microphysics and aerosol indirect effects in the global climate model ECHAM5-HAM. *Atmospheric Chemistry and Physics*, *7*, 3425–3446. https://doi.org/10.5194/acp-7-3425-2007

Mann, J. A. L., Chiu, J. C., Hogan, R. J., O'Connor, E. J., L'Ecuyer, T. S., Stein, T. H. M., & Jefferson, A. (2014). Aerosol impacts on drizzle properties in warm clouds from ARM Mobile Facility maritime and continental deployments. *Journal of Geophysical Research*, *119*, 4136–4148. https://doi.org/10.1002/2013JD021339

Marchand, R., Mace, G. G., Ackerman, T., & Stephens, G. (2008). Hydrometeor detection using Cloudsat—An Earth -orbiting 94-GHz cloud radar. *Journal of Atmospheric and Oceanic Technology*, *25*(4), 519–533. https://doi.org/10.1175/2007JTECHA1006.1

Michibata, T., Suzuki, K., Sato, Y., & Takemura, T. (2016). The source of discrepancies in aerosol–cloud–precipitation interactions between GCM and A-Train retrievals. *Atmospheric Chemistry and Physics*, *16*(23), 15413–15424. https://doi.org/10.5194/acp-16-15413-2016

Michibata, T., & Takemura, T. (2015). Evaluation of autoconversion schemes in a single model framework with satellite observations. *Journal of Geophysical Research: Atmospheres*, *120*, 9570–9590. https://doi.org/10.1002/2015JD023818

Morrison, H., & Gettelman, A. (2008). A new two-moment bulk Stratiform cloud microphysics scheme in the community atmosphere model, version 3 (CAM3). Part I: Description and numerical tests. *Journal of Climate*, *21*(15), 3642–3659. https://doi.org/10.1175/2008JCLI2105.1

Nakajima, T. Y., Suzuki, K., & Stephens, G. L. (2010). Droplet growth in warm water clouds observed by the A-Train. Part II: A multisensor view. *Journal of the Atmospheric Sciences*, *67*(6), 1897–1907. https://doi.org/10.1175/2010JAS3276.1

Penner, J. E., Quaas, J., Storelvmo, T., Takemura, T., Boucher, O., Guo, H., … Seland, Ø. (2006). Model intercomparison of indirect aerosol effects. *Atmospheric Chemistry and Physics*, *6*(11), 3391–3405. https://doi.org/10.5194/acp-6-3391-2006

Pincus, R., & Baker, M. B. (1994). Effect of precipitation on the albedo susceptibility of clouds in the marine boundary layer. *Nature*, *372*(6503), 250–252. https://doi.org/10.1038/372250a0

Platnick, S., Ackerman, S. A., King, M. D., Meyer, K., Menzel, W. P., Holz, R. E., … Yang, P. (2015). MODIS atmosphere L2 cloud product (06_L2), NASA MODIS Adaptive Processing System, Goddard Space Flight Center. https://doi.org/10.5067/MODIS/MOD06_L2.006

Quaas, J., Ming, Y., Menon, S., Takemura, T., Wang, M., Penner, J. E., … Schulz, M. (2009). Aerosol indirect effects—General circulation model intercomparison and evaluation with satellite data. *Atmospheric Chemistry and Physics*, *9*(22), 8697–8717. https://doi.org/10.5194/acp-9-8697-2009

Roh, W., & Satoh, M. (2014). Evaluation of precipitating hydrometeor parameterizations in a single-moment bulk microphysics scheme for deep convective systems over the tropical Central Pacific. *Journal of the Atmospheric Sciences*, *71*(7), 2654–2673. https://doi.org/10.1175/JAS-D-13-0252.1

Satoh, M., Matsuno, T., Tomita, H., Miura, H., Nasuno, T., & Iga, S. (2008). Nonhydrostatic Icosahedral Atmospheric Model (NICAM) for global cloud resolving simulations. *Journal of Computational Physics*, *227*(7), 3486–3514. https://doi.org/10.1016/j.jcp.2007.02.006

Satoh, M., Roh, W., & Hashino, T. (2016). *Evaluations of clouds and precipitations in NICAM using the Joint Simulator for Satellite Sensors*, *CGER's Supercomputer Monograph Report* (Vol. 22, p. 110). Tsukuba, Japan: Center for Global Environment Research.

Satoh, M., Tomita, H., Yashiro, H., Miura, H., Kodama, C., Seiki, T., … Kubokawa, H. (2014). The Non-hydrostatic Icosahedral Atmospheric Model: Description and development. *Progress in Earth and Planetary Science*, *1*(1), 18. https://doi.org/10.1186/s40645-014-0018-1

Sorooshian, A., Feingold, G., Lebsock, M. D., Jiang, H., & Stephens, G. L. (2009). On the precipitation susceptibility of clouds to aerosol perturbations. *Geophysical Research Letters*, *36*, L13803. https://doi.org/10.1029/2009GL038993

Sorooshian, A., Wang, Z., Feingold, G., & L'Ecuyer, T. S. (2013). A satellite perspective on cloud water to rain water conversion rates and relationships with environmental conditions. *Journal of Geophysical Research*, *118*, 6643–6650. https://doi.org/10.1002/jgrd.50523

Stephens, G. (2005). Cloud feedbacks in the climate system: A critical review. *Journal of Climate*, *18*(2), 237–273. https://doi.org/10.1175/JCLI-3243.1

Stephens, G. L., L'Ecuyer, T., Forbes, R., Gettlemen, A., Golaz, J. C., Bodas-Salcedo, A., … Haynes, J. (2010). Dreary state of precipitation in global models. *Journal of Geophysical Research*, *115*, D24211. https://doi.org/10.1029/2010JD014532

Stephens, G. L., Vane, D. G., Tanelli, S., Im, E., Durden, S., Rokey, M., … Marchand, R. (2008). CloudSat mission: Performance and early science after the first year of operation. *Journal of Geophysical Research*, *113*, D00A18. https://doi.org/10.1029/2008JD009982

Suzuki, K., Golaz, J. C., & Stephens, G. L. (2013). Evaluating cloud tuning in a climate model with satellite observations. *Geophysical Research Letters*, *40*(16), 4464–4468. https://doi.org/10.1002/grl.50874

Suzuki, K., Nakajima, T. Y., & Stephens, G. L. (2010). Particle growth and drop collection efficiency of warm clouds as inferred from joint CloudSat and MODIS observations. *Journal of the Atmospheric Sciences*, *67*(9), 3019–3032. https://doi.org/10.1175/2010JAS3463.1

Suzuki, K., Stephens, G. L., Bodas-Salcedo, A., Wang, M., Golaz, J.-C., Yokohata, T., & Tsuyoshi, K. (2015). Evaluation of the warm rain formation process in global models with satellite observations. *Journal of the Atmospheric Sciences*, *72*(10), 3996–4014. https://doi.org/10.1175/JAS-D-14-0265.1

Takahashi, H., Lebsock, M., Suzuki, K., Stephens, G., & Wang, M. (2017). An investigation of microphysics and subgrid-scale variability in warm-rain clouds using the A-Train observations and a multiscale modeling framework. *Journal of Geophysical Research: Atmospheres*, *122*(14), 7493–7504. https://doi.org/10.1002/2016JD026404

Tripoli, G. J., & Cotton, W. R. (1980). A numerical investigation of several factors contributing to the observed variable intensity of deep convection over south Florida. *Journal of Applied Meteorology*, *19*(9), 1037–1063. https://doi.org/10.1175/1520-0450(1980)019%3C1037:ANIOSF%3E2.0.CO;2

Wang, M., Ghan, S., Liu, X., L'Ecuyer, T., Zhang, K., Morrison, H., … Penner, J. (2012). Constraining cloud lifetime effects of aerosols using A-Train satellite observations. *Geophysical Research Letters*, *39*, L15709. https://doi.org/10.1029/2012GL052204

Watanabe, M., Suzuki, T., O'ishi, R., Komuro, Y., Watanabe, S., Emori, S., … Kimoto, M. (2010). Improved climate simulation by MIROC5: Mean states, variability, and climate sensitivity. *Journal of Climate*, *23*(23), 6312–6335. https://doi.org/10.1175/2010JCLI3679.1

Webb, M., Senior, C., Bony, S., & Morcrette, J. J. (2001). Combining ERBE and ISCCP data to assess clouds in the Hadley Centre, ECMWF and LMD atmospheric climate models. *Climate Dynamics*, *17*, 905–922. https://doi.org/10.1007/s003820100157

Yukimoto, S., Adachi, Y., Hosaka, M., & Sakami, T. (2012). A new global climate model of the meteorological research institute: MRI-CGCM3—Model description and basic performance. *Journal of the Meteorological Society of Japan*, *90A*(0), 23–64. https://doi.org/10.2151/jmsj.2012-A02

Yukimoto, S., Yoshimura, H., Hosaka, M., Sakami, T., Tsujino, H., Hirabara, M., … Kitoh, A. (2011). Meteorological Research Institute Earth System Model Version 1 (MRI-ESM1)—Model Description—. Tech. Rep. of MRI. (Vol. 64, p. 83). Tsukuba, Japan: Meteorological Research Institute. https://doi.org/10.11483/mritechrepo

Zhang, K., O'Donnell, D., Kazil, J., Stier, P., Kinne, S., Lohmann, U., … Feichter, J. (2012). The global aerosol-climate model ECHAM-HAM, version 2: Sensitivity to improvements in process representations. *Atmospheric Chemistry and Physics*, *12*(19), 8911–8949. https://doi.org/10.5194/acp-12-8911-2012

Zhang, Y., Klein, S. A., Boyle, J., & Mace, G. G. (2010). Evaluation of tropical cloud and precipitation statistics of Community Atmosphere Model version 3 using CloudSat and CALIPSO data. *Journal of Geophysical Research*, *115*, D12205. https://doi.org/10.1029/2009JD012006

Zhao, M., Golaz, J., Held, I., Ramaswamy, V., Lin, S., Ming, Y., … Guo, H. (2016). Uncertainty in model climate sensitivity traced to representations of cumulus precipitation microphysics. *Journal of Climate*, *29*(2), 543–560. https://doi.org/10.1175/JCLI-D-15-0191.1